



LiDARMarker: Machine-friendly Road Markers for Smart Driving Systems

Fengxu Yang

yangfx@shanghaitech.edu.cn

School of Information Science and Technology
ShanghaiTech University
Shanghai, China

Jiaqi Zhou

zhoujq2024@shanghaitech.edu.cn

School of Information Science and Technology
ShanghaiTech University
Shanghai, China

Zaizhou Yang

yangzzh@shanghaitech.edu.cn

School of Information Science and Technology
ShanghaiTech University
Shanghai, China

Zhice Yang*

yangzhc@shanghaitech.edu.cn

School of Information Science and Technology
ShanghaiTech University
Shanghai, China

Abstract

As assisted and autonomous driving systems become more prevalent, the need for accurate interpretation of road traffic signs is critical for driving safety and functionality. Current camera-based recognition methods face challenges due to the variability of traffic signs and environmental conditions, leading to potential inaccuracies. To address this, we propose LiDARMarker, a type of machine-readable traffic sign using infrared materials, making it invisible to human drivers but detectable by LiDAR-equipped vehicles. This paper introduces the design, fabrication, and efficient decoding methods of LiDARMarker. LiDARMarker is tailored to the emerging capabilities and needs of modern vehicles, enhancing their ability and accuracy in traffic sign recognition while avoiding interference with human drivers. Through the proposal of LiDARMarker, we aim to inspire the rethinking of the design of traffic sign systems in the context of modern vehicles.

CCS Concepts

- **Hardware → Sensor applications and deployments; Sensor devices and platforms; Sensors and actuators.**

Keywords

Autonomous Driving, LiDAR, Traffic Sign, Machine-friendly Marker, IR Absorbing Material

ACM Reference Format:

Fengxu Yang, Zaizhou Yang, Jiaqi Zhou, and Zhice Yang. 2025. LiDARMarker: Machine-friendly Road Markers for Smart Driving Systems. In *The 23rd ACM Conference on Embedded Networked Sensor Systems (SenSys '25)*, May

*Corresponding Author



This work is licensed under a Creative Commons Attribution-NonCommercial 4.0 International License.

SenSys '25, May 6–9, 2025, Irvine, CA, USA

© 2025 Copyright is held by the owner/author(s).

ACM ISBN 979-8-4007-1479-5/25/05

<https://doi.org/10.1145/3715014.3722083>

6–9, 2025, Irvine, CA, USA. ACM, New York, NY, USA, 13 pages. <https://doi.org/10.1145/3715014.3722083>

1 Introduction

Recently, assisted and autonomous driving systems (ADS) have been increasingly integrated into modern vehicles [42]. ADS enables vehicles to perceive their surrounding environment and make control decisions, either to assist the driver (in critical situations) or to achieve autonomous driving. Advanced ADS relies on a range of intelligent technologies, such as pedestrian and vehicle recognition, lane detection, route planning, and more [27]. Among these, the ability to accurately interpret road traffic signs, *i.e.*, pavement markings and road signs, is essential to its core functionalities. These markers not only provide necessary navigation information but also indicate important driving regulations, serving as the foundation for safe driving.

Currently, ADS primarily relies on two methods to acquire road traffic sign information. One method involves using the vehicle's location to retrieve information from digital maps [5]. However, due to the limited coverage of high-precision maps and the accuracy of localization technology, this method has limitations in both granularity and precision. Therefore, a more generalized approach is to incorporate vehicle cameras to capture and recognize traffic signs in real-time through computer vision algorithms [13].

Over the past few years, substantial efforts have been made by both academia and industry to improve camera-based sign recognition accuracy [24]. However, this method still struggles with the complexity arising from the diversity and variability of traffic signs and environmental conditions. Current recognition algorithms are trained on limited datasets, and while most road traffic signs fall within the feature range depicted by these datasets, there are inevitably out-of-range cases in real-world scenarios, such as construction zones [36], rural roads [1], and private roads [35]. Even standard traffic signs cannot be guaranteed to be correctly recognized under conditions like bad weather, complex lighting, or when the signs are damaged or aged.

One major cause of these issues lies in the fact that the primary target of current traffic signs is human drivers. To convey necessary information quickly and with minimal cognitive overhead during

driving, the content of these signs is often designed to be as human-friendly as possible, e.g., symbols or simplified text. However, this design is not fully aligned with the preferred information formats for machine vision. These signs are not only difficult to distinguish from the physical environment but also lack prominence, or are even deficient, in many key properties of information delivery, such as information density, signal contrast, and error correction capabilities. But what if machine-friendly traffic signs, e.g., using a structured binary image similar to barcodes, were added to the current road environment? Traffic regulations strictly limit the density and usage conditions of traffic signs, not to mention that such attempts could lead to barcode signs competing with existing signs and distracting the driver's visual attention.

The traditional design of road traffic signs is driver-centric, but with the rapid development of ADS, we believe it is time to reassess this philosophy. If traffic signs could provide more efficient and accurate information to ADS systems, it could effectively enhance the functionality and safety of modern driving. As such, we envision that modernized traffic signs should not only cater to the capabilities and needs of drivers but also to those of ADS-equipped vehicles. Specifically, they should be machine-friendly while avoiding visual interference with driver. Additionally, from a practical perspective, they should allow for smooth deployment and maintenance.

To meet these requirements, we propose a type of traffic sign called LiDARMarker, a specialized barcode dedicated for the driving environment. Unlike traditional traffic signs that reflect visible light to convey information, the content of LiDARMarker is made using visual-transparent and infrared-absorbing materials, making it invisible to the human eye. It can be overlaid as a transparent coating on top of traditional traffic signs or applied to any blank surfaces, such as buildings and roadways. To vehicles, LiDARMarker's content is revealed through the images captured by its LiDAR, not by the camera. LiDAR is a widely used distance measurement and long-range imaging sensor in modern ADS vehicles. Since LiDAR uses infrared (IR) lasers for active sensing, its imaging data will include changes caused by the IR content of LiDARMarker. The ADS can extract the marker's information using its LiDAR data.

As shown in Fig. 1, LiDARMarker is a structured 2D graphical code similar to barcodes, but LiDARMarker faces issues that differ from known barcodes. LiDARMarker is not intended to be captured by cameras; instead, it is presented in LiDAR point cloud. This introduces a series of unique challenges. Firstly, the reason for LiDARMarker sector-like shape is to ensure that the marker can be reliably decoded from sparse point cloud data, addressing the limitations of standard barcodes, which are often ineffective at conveying directional information. The sector shape allows LiDARMarker to provide both positional and directional cues, which are crucial for orientation estimation within the 3D space represented by LiDAR data. Secondly, processing point clouds with millions of data points introduces substantial computational demands. An easily recognizable marker structure is specifically designed to facilitate quick and efficient extraction, reducing the computational load required to locate and decode the marker amidst large volumes of point cloud data. This optimization is essential for real-time applications, where fast processing is critical to maintaining performance.

We implement LiDARMarker in a real-world traffic environment and evaluate its performance under practical conditions. The results

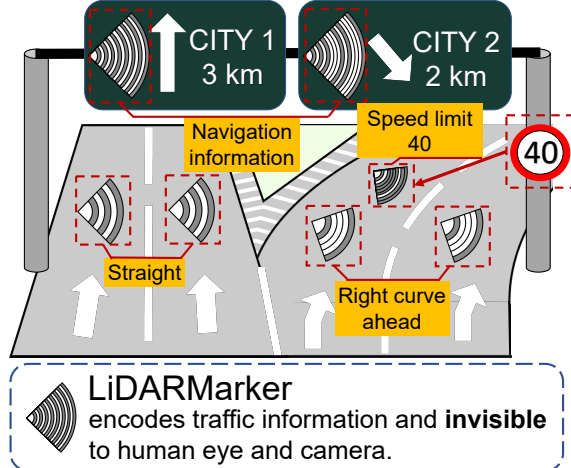


Figure 1: LiDARMarker assists LiDAR-equipped vehicles to better perceive traffic sign. The LiDARMarker is applied to pavement surfaces to guide LiDAR-based vehicles, remaining invisible to the human eye while detectable by LiDAR.

demonstrate that LiDARMarker, leveraging its innovative marker design and decoding pipeline, can effectively assist LiDAR-equipped vehicles in obtaining navigation information within a 15-meter range, operating at a frame rate of 60 Hz. We believe that LiDARMarker can serve as a valuable addition to the current traffic sign system, offering a new and efficient way to convey critical information to ADS while preserving the aesthetic and functional integrity of existing road infrastructure. To summarize, this paper makes the following contributions:

- We propose LiDARMarker, a novel, invisible navigational marker system specifically designed for LiDAR-equipped vehicles. LiDARMarker is engineered to be machine-friendly, undetectable by human vision, and seamlessly compatible with existing traffic signage.
- We design a sector-shaped barcode marker structure that is optimized for easy detection and decoding from LiDAR point cloud data. The unique shape and layout of the marker allow for efficient extraction and decoding, ensuring real-time performance even in dense traffic environments.
- We implement LiDARMarker and conduct extensive evaluations in a practical traffic environment, testing the system's overall performance in terms of detection capability, decoding accuracy, and real-time processing efficiency. The results show that LiDARMarker can assist ADS-equipped vehicles in obtaining accurate navigation information, enabling real-time operations.

2 Prior Knowledge

In ADS scenarios, the distance to environmental objects is an important factor to consider when making control decisions [21]. Among various distance sensing methods, the LiDAR sensor stands out with advantages in detection range, accuracy, spatial resolution, and robustness to dynamic lighting conditions [46]. With the rapid decrease in manufacturing costs, the global market saw a shipment of automotive LiDAR sensors reaching 0.7 million units in 2023 [41],

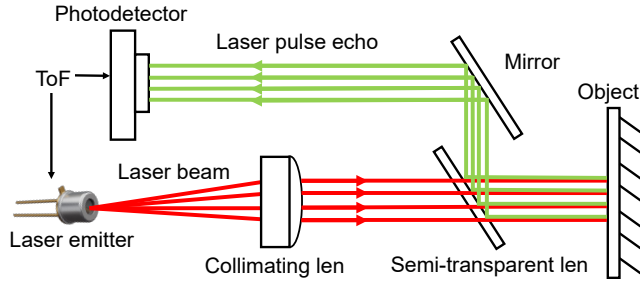


Figure 2: LiDAR ranging principle.

with an expected growth rate of 19.5% in 2024 [38]. LiDAR has become a common sensor in new vehicles, especially those equipped with advanced ADS. LiDARMarker works with LiDAR sensors, so in this section, we will introduce the LiDAR working principle.

2.1 LiDAR Ranging Principle

LiDAR utilizes the time-of-flight (ToF) mechanism to measure distance [22]. As illustrated in Fig. 2, the key components of LiDAR include a laser pulse emitter and a photodetector. During distance measurement, a portion of the energy from the laser pulse emitted by the emitter is reflected by objects in the environment and returned, then the photodetector records the time delay t of the echo pulse relative to the emitted pulse. The distance to the object can then be determined using the formula $d = t \times c/2$, where c is the speed of light.

In automotive applications, the operating wavelength of LiDAR's laser emitter is generally chosen from 905 nm or 1550 nm [14, 32]. These wavelengths fall within the IR spectrum, which is invisible to the human eye. One advantage of this design is that it avoids light interference with pedestrians and other drivers when the LiDAR is in operation. However, invisibility does not imply that it poses no risk to the human eye's photoreceptor cells. Due to eye safety concerns, IR lasers are subject to strict power limitations. By using highly sensitive photodetectors, such as avalanche photodiodes [17], a typical ranging distance of over 200 meters can be achieved [14, 32]. It is worth noting that light-based ToF ranging does not necessarily require lasers as the light source; however, laser beams have high directionality, which maximizes the ranging distance under limited power conditions.

2.2 LiDAR Imaging Principle

A clear advantage of LiDAR compared to radio frequency and acoustic radar is its ability to provide image-level resolution for object distance information. This is achieved by extending the single-point ranging mechanism shown in Fig. 2 into the spatial domain: controlling the laser beam to perform high-speed 2-dimensional scanning, generating continuous distance measurements of the surrounding environment. By considering the scanning angle of the laser beam and the corresponding distance information, the 3-dimensional position of each reflection point in space can be obtained, resulting in a *3D Point Cloud*.

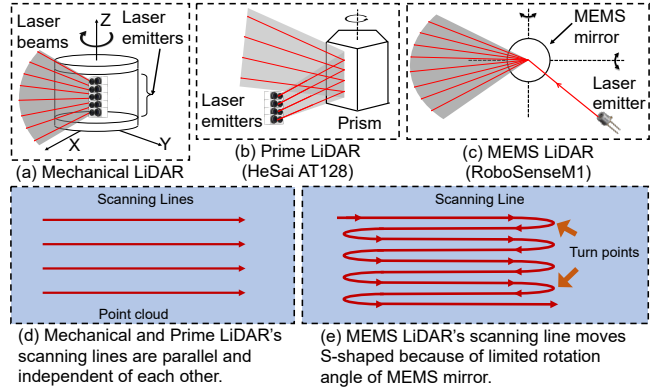


Figure 3: Different LiDAR scanning mechanisms.

LiDAR scanning can be implemented in various ways, and different scanning methods result in different point cloud timing sequences and data structures, which are closely related to the efficiency of point cloud processing [26]. Early LiDAR systems use a mechanical rotating structure [31], where the emitter and detector in Fig. 2 rotate as a whole to measure different positions. An example is shown in Fig. 3(a). A rotor is used to carry multiple stacked laser emitters and detectors, allowing a column of beams to measure each time. When the rotor rotates by a degree, the position of this column of beams scans accordingly, thereby covering the entire Field of View (FoV), as shown in Fig. 3(d). We refer to the set of 3D points measured by the same detector as a *scanning line*. For example in Fig. 3(d), the points on each horizontal line belong to the same scanning line.

The mechanical LiDAR has a simple structure, but it comes with the drawbacks of high cost and a large form factor. More integrated solutions using built-in prisms and Micro-Electro-Mechanical System (MEMS) mirrors have been developed, rapidly replacing mechanical LiDAR in ADS [23]. Fig. 3(b) and Fig. 3(c) provide two examples. The prism LiDAR simplifies the scanning structure by using a rotating prism mirror to reflect the laser beams instead of rotating the laser emitters. Its scanning line structure is similar to that of mechanical LiDAR. In Fig. 3(c), the MEMS LiDAR uses a MEMS mirror capable of 2D oscillation to reflect the laser beams [30]. The left-right oscillation of the MEMS mirror allows the reflected laser beams to scan back and forth horizontally, and by adding a suitable (slow) vertical oscillation, it can further span the left-right scanning to achieve 2D spatial scanning in both horizontal and vertical directions. Fig. 3(e) shows MEMS LiDAR can cover an entire area using just a single laser beam, the points forming the entire zigzag pattern belong to the same scanning line.

3 Motivation

ADS relies on multiple channels to obtain or confirm road traffic information because no single channel can perfectly guarantee accurate acquisition. Consulting digital maps not only depends on precise and timely-updated map information but also requires accurate vehicle location data, which cannot be fully guaranteed with current localization technologies. Vehicle localization primarily based on satellite navigation faces challenges such as location drift and inaccurate altitude in complex mountainous and urban

environments. Scenarios such as multi-branch tunnels, large interchanges, and complex overpasses are common situations where accurate vehicle localization is difficult to ensure. Additionally, in non-urban areas, the timeliness of digital maps is often a more pronounced issue.

Camera-based visual methods can recognize road traffic signs in real-time, providing important supplementary information for ADS. However, current road traffic signs are human-centric, using symbols and simple text as the medium for information expression. Vision algorithms based on statistical information may not effectively cover content with highly arbitrary features; for example, customized signs outside of the training set may appear in some areas. Furthermore, cameras utilize reflected environmental light from objects for imaging. In low-light conditions, such as heavy rain and nighttime, or in situations with dynamic changes in ambient light, such as entering or exiting tunnels, the imaging quality is affected, which impacts recognition results.

To this end, we believe that additional mechanisms should be developed to further enhance the redundancy of the ADS's information acquisition capabilities, which is particularly important for achieving large-scale autonomous driving in the near future. There are many possible design choices to address some of the limitations mentioned above, such as adopting radio markers, intelligent visible light markers, and improved vehicle localization methods. While we do not oppose these methods—since safety redundancy can never be excessive—we hope to find a solution that is both smooth in deployment and low in maintenance costs. Thus, we conducted this research to design a new road traffic marker system, LiDARMarker, with the following desirable properties:

- (1) Machine-friendly information carrier. LiDARMarker is a structured graphical encoding method similar to a barcode. It uses high-contrast binary patterns to encode information and has a well-defined symbol space, allowing for fast, efficient, error-detectable, and prior-knowledge-agnostic decoding algorithms.
- (2) Invisible to humans and cameras. LiDARMarker's encoded content is physically expressed using infrared optical materials, which are nearly transparent in the visible light spectrum. Thus, overlaying LiDARMarker on existing sign panels or deploying new LiDARMarker markers will not interfere with current road traffic signs or affect the aesthetics of buildings and roads.
- (3) Good adaptability to lighting conditions. The encoded content of LiDARMarker is expected to be captured in the vehicle's LiDAR point cloud. LiDAR illuminates and images the environment using its laser pulses, making it insensitive to ambient light changes.
- (4) Easy maintenance. LiDARMarker's encoded content can be encapsulated as a transparent overlay within ordinary traffic sign panels or applied to the road surface with transparent adhesive materials. To combat aging and damage, it requires periodic maintenance measures similar to those for current traffic signs.
- (5) Easy vehicle deployment. For LiDAR-equipped vehicles, decoding LiDARMarker only requires an update to its ADS software.



Figure 4: Undiluted infrared absorbing material.

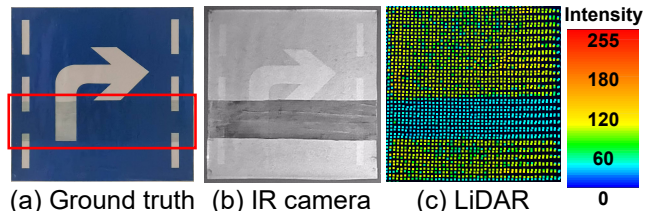


Figure 5: IR-absorbing coating absorbs IR energy, reducing the brightness in IR cameras and the intensity in LiDAR.

4 Marker Design

4.1 IR Absorbing Materials

In this section, we introduce the infrared (IR) absorbing materials used in the marker design, discussing their properties and how they affect the LiDAR-generated point cloud. Following this, we demonstrate how these properties are utilized to create an effective marker pattern.

4.1.1 Property of IR Absorbing Materials. As its name suggests, the material's primary function is to absorb IR light. Many materials, such as graphite or even black printer paper, can absorb IR, but they are unsuitable for our marker design as they are visible to the human eye. To avoid visual interference in driving situations, we repurpose a type of window glass coating originally developed for heat retention in buildings, as shown in Fig. 4. This coating contains metal nanoparticles, such as antimony tin oxide (ATO) and indium tin oxide (ITO), which give the undiluted coating a deep blue hue. The coating absorbs IR light with about 80% efficiency while transmitting approximately 90% of visible light at a thickness of 5 to 10 micrometers. This combination of high IR absorption and high visible-light transmittance makes it ideal for our marker, allowing it to remain “invisible” to the human eye while still being detectable in LiDAR point clouds.

To illustrate this effect more clearly, we demonstrate the impact of the IR-absorbing coating on traffic signs in both the visible light and IR light domains, as shown in Fig. 5¹. In Fig. 5(a), a strip of IR-absorbing coating is applied to a traffic sign, highlighted by the red box. In the RGB image, the traffic sign remains clearly visible through the coating, allowing drivers to read the sign's information without obstruction.

However, in Fig. 5(b), captured by an IR camera, a noticeable difference in reflected IR light brightness is observed between the

¹The RGB and IR images were captured using a DUMU RGB-IR camera [9], and the point cloud data was captured using a Robosense M1 LiDAR [32].

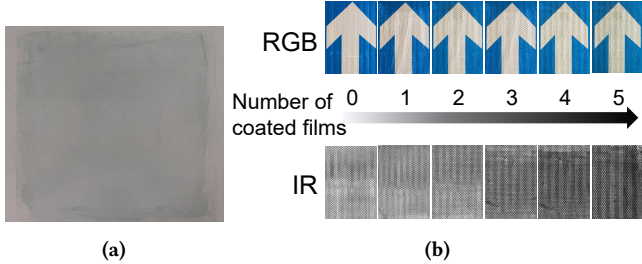


Figure 6: (a) A plastic film coated with an IR-absorbing layer. (b) The visibility of RGB camera v.s. IR camera.

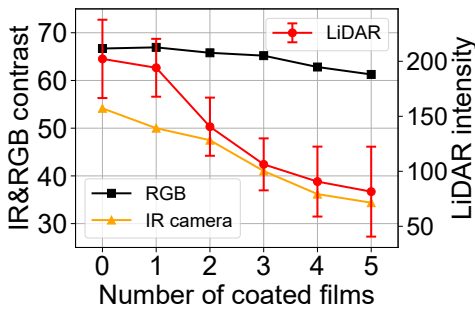


Figure 7: The trend of IR and RGB contrast, as well as LiDAR intensity, when applying different numbers of films to a traffic sign.

coated and uncoated areas. The region with IR-absorbing coating appears darker. Similarly, in the LiDAR point cloud data shown in Fig.5(c), the coated strip exhibits lower intensity than the uncoated areas. This contrast in intensity allows information to be encoded within the point cloud without affecting human visibility, making the IR-absorbing coating an effective and non-intrusive marker for LiDAR-based navigation.

We note that Fig. 5(a) is specifically designed to highlight differences in the visible light domain by applying an undiluted coating with a thicker layer. However, in practical applications, a diluted coating and thinner coating layers are used to ensure that the coating remains invisible to the human eye. To study the visibility of IR-absorbing coatings with varying thicknesses, we conducted an experiment, as shown in Fig.6. We used a plastic film coated with an IR-absorbing layer approximately 5 μm thick, as depicted in Fig.6(a), and then stacked multiple layers of this film onto a sign featuring a reflective coating (Fig.6(b)).

We subsequently measured the contrast in the RGB and IR images, as displayed in Fig. 7. The results show that, as the number of coated film layers increases, the decrease in RGB contrast is more significant than the drop in IR contrast. Since the human eye's minimum detectable contrast ranges between 0.5% and 2%, the traffic sign remains readable to both the human eye and RGB cameras, but lower contrast affects the clarity of the IR camera image. Additionally, we examined the LiDAR intensity under the same conditions, as indicated by the red trend in Fig. 7. As the coating thickens, the LiDAR intensity exhibits a similar decline to that observed in the IR camera.

Conclusion: We introduced an IR-absorbing coating and demonstrated its effects on RGB cameras, IR cameras, and LiDAR. When

applied to an object, this coating reduces reflected IR energy in the coated areas while preserving the object's visible appearance. This property enables the embedding of navigational information into LiDARMarker without affecting human vision or the readability of traffic signs.

4.2 Marker Symbolology

Numerous markers have been designed and can be categorized into two main types: 1) one-dimensional (1D) barcodes, such as linear barcodes, and 2) two-dimensional (2D) barcodes, such as quick response codes (QR codes). Some works have adapted these markers for use with LiDAR sensors, including calibration boards [3] and VR applications [18]. However, these approaches rely on 2D image processing mechanisms, which fail to fully exploit LiDAR's unique imaging properties and scanning mechanism. This leads to inefficiencies and limits their real-time performance. In this section, we analyze the shortcomings of existing markers and introduce our marker design.

4.2.1 Design Choice. The linear barcode is a type of 1D marker, representing data using a combination of black bars and white spaces. However, two key challenges prevent their direct use in LiDAR processing.

First, the encoding mechanism of barcodes relies on bar-width ratios, which require LiDAR to detect the narrowest bar and accurately measure relative widths. For example, the symbol "A" in Code-128 [10] encodes widths as "111323". Only by accurately measuring the width of "1" can the width of 2 and 3 be measured. However, LiDAR's resolution limitations may prevent detection of the narrowest bar, causing decoding failures. Second, barcodes lack orientation information, which is critical in traffic scenarios for determining driving direction. For instance, vehicles must identify a marker's orientation on the road surface to navigate correctly. Consequently, reliance on bar-width ratios and the absence of orientation cues make linear barcodes unsuitable for LiDAR processing in traffic applications.

A 2D barcode, also known as a matrix barcode, encodes information both horizontally and vertically, offering greater data capacity compared to linear barcodes. The most well-known example is the QR code, which consists of black squares arranged on a white background. However, 2D barcodes still face similar resolution challenges as their 1D counterparts.

Fig. 8 illustrates four types of 2D barcodes captured in a LiDAR point cloud from a distance of 6.7 m. At this distance, the boundaries of individual black squares cannot be accurately measured, resulting in blurry edges and making decoding difficult. Decoding a 2D barcode requires each LiDAR point to correspond precisely to a square in the barcode. However, due to laser beam aperture effects and sampling errors, the measured intensity can deviate from the actual value, causing the distinction between black and white squares to become blurred. This inherent limitation makes 2D barcode decoding challenging and error-prone. Some approaches attempt to compensate by superimposing multiple frames to enhance resolution, but this sacrifices real-time performance.

Additionally, the orientation estimation of 2D barcodes relies on specialized patterns, such as the three squares in the corners of a QR code, which are protected by quiet zones under ideal conditions. In

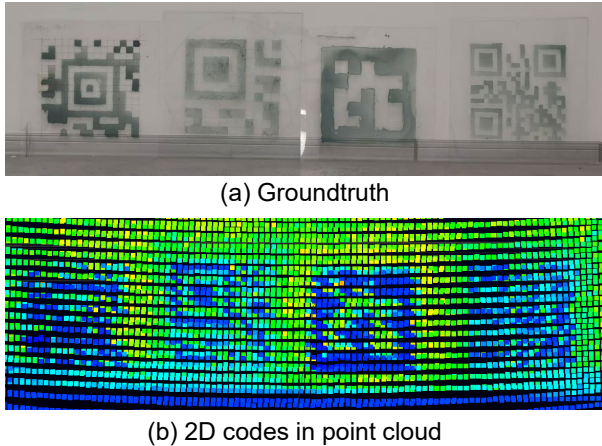


Figure 8: The four types of 2D codes in a point cloud. 2D codes are placed 6.7 m away from LiDAR.

real-world traffic environments, however, these patterns are often degraded or lost due to low LiDAR's resolution and noise.

Lastly, for traffic applications, traffic signs typically convey simple information, such as speed limits, stop commands, or directional indicators e.g., "Turn Left". The high information capacity of 2D barcodes is unnecessary for these use cases, making them overly complex to maintain and inefficient in practice. Therefore, we summarize the challenges of existing markers in LiDAR imaging systems as follows:

- Orientation estimation should not rely solely on specialized patterns within the marker.
- Binary encoding mechanisms must be robust to variations in distance and scanning angles.
- The marker design should be easily distinguishable from other objects and simple to maintain.

4.2.2 Marker Design. Fig.9(a) illustrates the marker structure of LiDARMarker, while Fig.9(b) presents the LiDAR view when the marker is applied to a pavement road surface with an IR-absorbing coating.

To address challenge 1), we replaced the approach of relying on specific patterns for orientation estimation with an unconventional quarter-circle sector outline. This design choice ensures that the marker is easily distinguishable from other traffic objects such as signs, road markings, and vehicles. For orientation decoding, the outline of the quarter-circle sector is extracted by fitting a curve to the LiDAR points cloud corresponding to the IR absorbing regions (details of this process are discussed in Sec.5). The quarter-circle sector comprises several concentric bars of equal width, each representing either a high-reflection bar (1) or a low-reflection bar (0). Low-reflection bars are coated with IR absorbing coating, as described in Sec.4.1.1, while high-reflection bars correspond to the road surface.

To address challenges 2) and 3), we utilize equal-width bars instead of the variable-width bars commonly used in linear barcodes. In variable-width designs, decoding depends on the narrowest bar, which may be feasible at close range with high-resolution cameras but becomes problematic in LiDAR systems with limited resolution

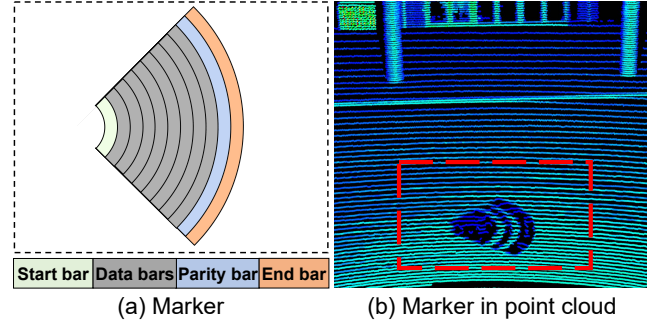


Figure 9: The LiDARMarker marker design and its LiDAR view when applied to a pavement road surface with an IR-absorbing coating.

(1200×128) and at longer distances. The inability to detect the narrowest bar effectively establishes a lower boundary for decoding the entire marker. By adopting equal-width bars, we mitigate this issue, reducing the barrel effect and increasing the probability of successful detection for each bar. For example, under the same total marker width and distance, equal-width bars are 1.57 times wider than the narrowest bar in a variable-width design encoded by Code-128. This makes equal-width bars significantly easier for LiDAR to detect, particularly in low-resolution or long-range scenarios. Since multiple scan lines may pass through the marker simultaneously, as long as one scan line contains all bars, a partially occluded marker will still function correctly.

4.2.3 Data Structure. The data structure of the bars consists of a start bar, data bars, a parity bar, and an end bar. The start and end bars are single low-reflective bars that serve two main functions: 1) they indicate the beginning and end of the data bar sequence for decoding, and 2) they provide a reference outline shape for orientation estimation.

The data bars can vary in length and are used to encode the traffic sign's information. The parity bar employs even parity to validate the integrity of the data bars. Notably, the data bars are not limited to an 8-bit capacity and can be extended to include more bars for encoding more information. However, an 8-bit capacity is sufficient for most traffic signs and pavement markers in practice. For instance, the US road symbol signs [11] define 184 traffic signs, and China defines 65 [48], both of which can be fully covered within an 8-bit system. This marker design is tailored to leverage the LiDAR's imaging properties and unique scanning mechanism, thereby reducing decoding overhead and enabling real-time marker decoding. Further details on marker detection and decoding are provided in Sec. 5.

5 Marker Detection and Decoding

5.1 Processing Point Cloud Data

Typically, LiDAR point cloud processing approaches fall into two main categories. The first category transforms the point cloud into a 2D image and then uses image processing techniques to detect the marker. The second category processes the data directly in 3D. However, these approaches often incur substantial computational

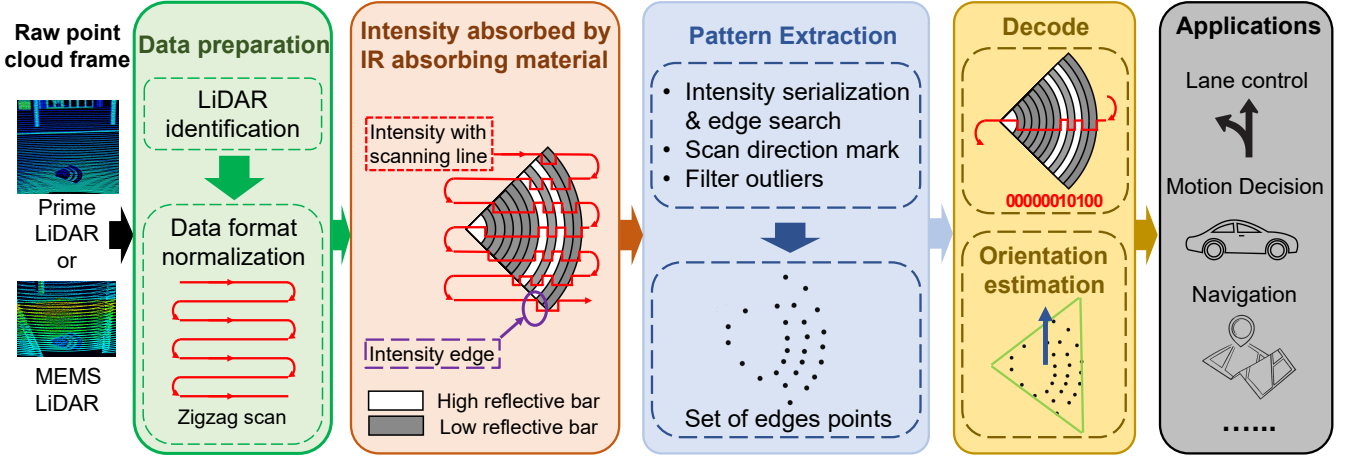


Figure 10: The pipeline of marker detection and decoding.

overhead. For instance, performing bird's-eye view transformations to be compatible with established 2D methods, accumulating point cloud data to mitigate LiDAR's low resolution, and clustering to recognize objects. They may also face additional drawbacks, including high overhead and reliance on specialized datasets, ultimately hindering real-time processing of large-scale point cloud data. Therefore, we propose a novel detection pipeline based on the LiDARMarker design, which detects the marker within the point cloud and decodes the navigation information. Inspired by signal processing concepts from communication systems, this pipeline arranges LiDAR scan lines into a series of points and processes them as signals.

5.2 Efficient Processing Method

Unlike existing image processing methods, our detection pipeline fully utilizes the LiDAR scanning mechanism. By exploiting the unique marker shape in the point cloud, we construct a deterministic process for marker extraction, decoding, and orientation estimation. As shown in Fig. 10, the pipeline comprises three main steps: 1) data preparation, 2) pattern extraction, and 3) decoding and orientation estimation. Notably, the pipeline is designed for single-frame processing to ensure real-time performance. Accordingly, the input is a single point cloud frame, and the output is the decoded marker together with its orientation in that frame.

5.2.1 Data preparation. In this step, our goal is to normalize different LiDAR data formats. First, we identify the LiDAR model from the attributes of the point cloud and use this as a basis to initialize the corresponding radar parameter settings, such as angular resolution. Next, we normalize the data structure according to different scanning methods. For prism-based LiDAR, the data format is the same as that of mechanical radar, their scan lines are in the same direction, as described in Fig. 3(d). In contrast, MEMS radar spans the zigzag scanning to achieve 2D spatial scanning in both horizontal and vertical directions as shown in Fig. 3(e). To maintain a consistent data format, we arrange the prism LiDAR's point cloud in a serpentine sequence, effectively emulating the MEMS LiDAR's

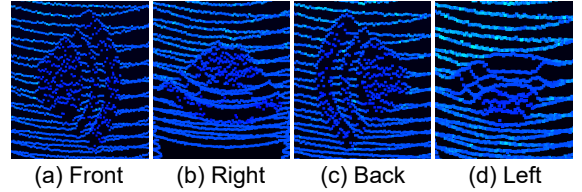


Figure 11: Examples of different orientations.

reciprocating scan by connecting the end of one scan line to the beginning of the next.

5.2.2 Pattern Extraction. In our marker pattern design, the high-reflective bar corresponds to the normal road surface, while the low-reflective bar indicates the marker's pattern. As illustrated in Fig. 10, when the LiDAR beam crosses the marker, the intensity of the point cloud exhibits a pronounced difference between the high-reflective and low-reflective bars.

To extract pattern of marker, we first serially arrange the point cloud data into a 1D signal benefited by previous step. Next, we apply a gradient method to identify all falling and rising intensity edges and then pair each falling edge with a corresponding rising edge in a one-to-one manner. Each edge pair thus contains one falling edge and one rising edge. Among these pairs, at least one set includes the complete bit stream. Since the reciprocating zigzag scan, there may be an inverted bit stream. To resolve this, we calculate the yaw angle for each point and classify it as left-to-right or right-to-left based on whether the yaw increases or decreases relative to the previous point. As defined earlier, left-to-right is the positive direction and right-to-left is the negative direction. During decoding, we use the scan direction to correct any inverted bit stream. We then apply filtering rules to discard outliers or edge pairs that are too short or too long and thus unlikely to belong to the marker. The remaining edge pairs, which may contain the encoded bit stream, are subsequently used to decode the marker and estimate its orientation in the next step.

5.2.3 Decode and Orientation Estimation. In this step, we decode the bit stream from each edge pair and estimate the marker's orientation. First, we extract the intensity of all LiDAR points lying

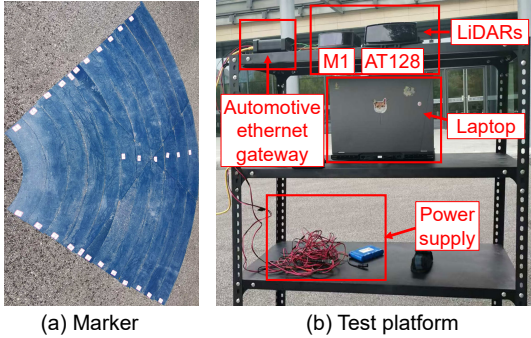


Figure 12: Implementation of marker and testbed.

between each pair of edges to form an intensity signal. Because segmentation thresholds can vary with distance and ground material, we employ a dynamic thresholding method to binarize the signal. Initially, a preset threshold is applied to segment the signal into predefined bars; each bar contains one or more occurrences of 0 or 1, and a voting mechanism determines whether the bar encodes a 0 or a 1. The resulting bit stream then undergoes parity verification. If it fails, we retry with different dynamic thresholds; if all thresholds fail, the corresponding edge pair is discarded. Successfully verified streams are recorded as potential candidates. Once all edge pairs have been processed, the most frequent bit stream among the candidates is selected as the final result. Finally, the coordinates derived from successfully decoded edge pairs are used to determine the spatial position of the marker, which is output together with the decoding and orientation results.

For orientation estimation, we first fit a minimum enclosing triangle to the marker outline extracted from edge pairs, clipping the Z-axis to reduce computational complexity. We then derive the orientation from the triangle as follows: 1) identifying the vertex with the smallest sum of sides, 2) calculating the vector sum of its two sides, and 3) computing the perpendicular vector as the marker's orientation. Because traffic signs only require coarse orientation accuracy, we divide directions into eight categories, e.g., front, back, left, right, front-left, front-right, back-left, and back-right, align the calculated orientation with the nearest category.

Please note that the quarter-circle shape of LiDARMarker supports decoding only when oriented between front-left and front-right. In other orientations, LiDAR scan lines cannot fully cover all bars. Fig. 11 illustrates examples: front, right, back, and left. Sparse point clouds and large scan line intervals fail to capture low-reflection bars in orientations like Fig. 11(b) and Fig. 11(d). While Fig. 11(c) is decodable, markers facing backward are irrelevant as they correspond to opposite-lane signs. Therefore, decoding results outside the front-left to front-right range are discarded to ensure only relevant data is used for navigation.

6 Evaluation

6.1 Evaluation Setup and Metrics

6.1.1 Setup. **Marker Fabrication.** LiDARMarker was originally designed to be printed directly on pavement surfaces. However, we chose to fabricate the marker on prefabricated acrylic panels for greater flexibility in experimentation because that large-scale road

Marker parameters	
Road surface	Asphalt
Bar width	0.15 m
Bars	11
Radius	2 m
Start bar offset	0.35 m
Encode bits	8 bits + 1 parity bit
Test code set	5,11,27,48,52,57,114,115,121,154,155,185,245

Table 1: Marker evaluation parameters.

LiDAR & Decoding parameters	
Installation height	1.6 m
LiDAR refresh rate	10 Hz
Angular resolution	0.2 degree
Preset threshold	8±1

Table 2: LiDAR and decoding evaluation parameters.

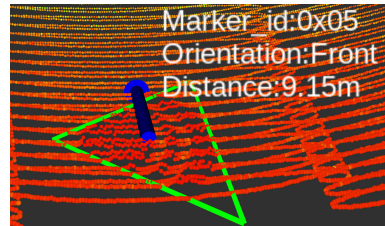


Figure 13: The results of LiDARMarker in RViz.

coating requires government approval. As shown in Fig. 12(a), the marker features all low-reflection bars coated with an IR-absorbing coating. Each bar is laser-cut into individual pieces for easy transportation and flexible setup. The marker has a 2-meter diameter and consists of 11 bars, encoding 8-bit of traffic sign information plus 1 parity bit. To facilitate testing, we prepared 13 unique encodings selected from the 8-bit encoding space, with a default encoding of 0x05 used in most evaluations.

LiDAR and Decoding. We used commercially available models, including the Robosense M1 [32] and Hesai AT128 [14], to simulate real-world applications. The M1 has a resolution of 128×600 points per frame, while the AT128 offers 128×1200. Due to its lower image quality, the M1 was primarily used to establish a performance baseline for LiDARMarker. LiDAR was mounted horizontally at 1.6 m, with a 10 Hz refresh rate and 0.2 degree angular resolution. LiDAR specifications are in Table 2. The point cloud data is captured via an automotive Ethernet gateway, converting it into standard Ethernet packets. Both the LiDAR and gateway are powered by a 12 V supply. The decoding pipeline, implemented in C++ on a laptop with an AMD 8-core CPU@4.5G Hz and 16 GB memory, runs under ROS2 Humble. Data is parsed into a PointCloud2 structure by LiDAR drivers and sent to the decoding algorithm node via ROS2 messages. For binary decoding, we use an intensity threshold of 8 ± 1 . Each test data consists of about 10 seconds of point cloud data, or 100 frames. All tests are conducted with default parameters unless specified otherwise.

Metrics. Four metrics evaluate frame-level performance: *Detection Rate* is defined as $R_{det} = \frac{N_{detected}}{N_{total}}$; *Correct Rate* is defined as $R_{corr} = \frac{N_{correctly\ decoded}}{N_{total}}$; *Decoding Time*, measured from frame publication to decoding output; *False Alarm Rate (FAR)*, the ratio of falsely detected markers to total non-marker frames.

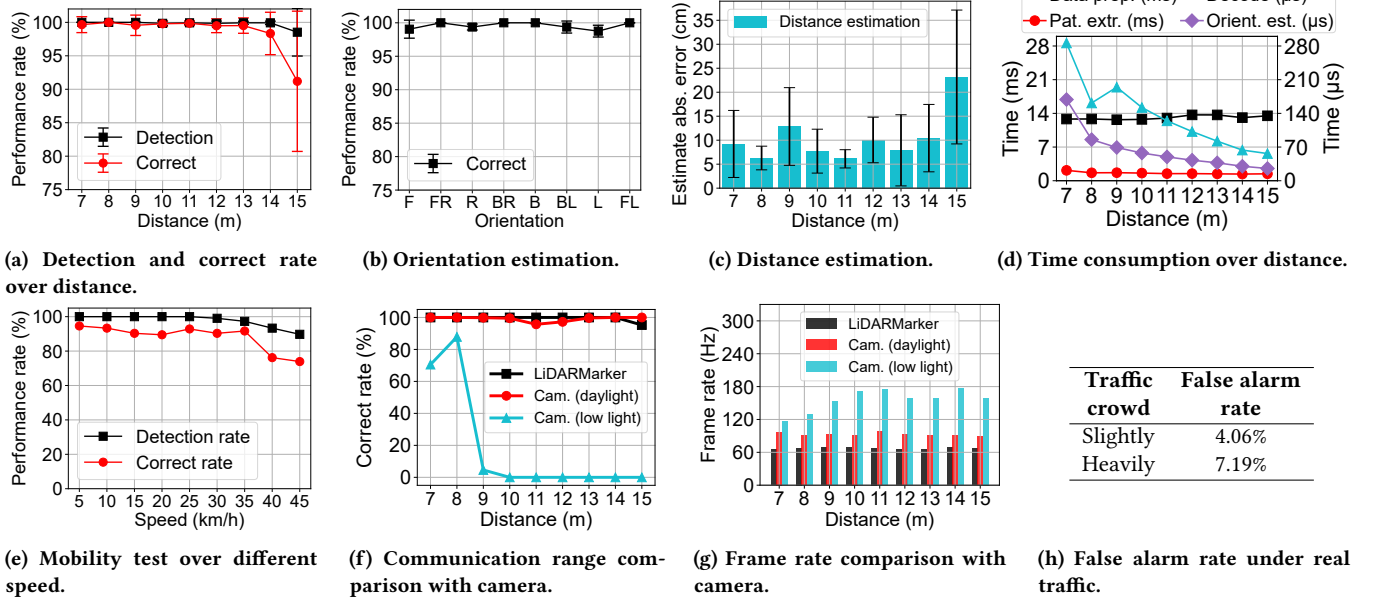


Figure 14: Overall performance of the LiDARMarker.

6.2 Evaluation Results

Fig. 13 shows the marker decoding and orientation estimation in RViz. The marker is outlined in green, with a blue arrow indicating orientation. IDs, orientation, and distance estimates are labeled, offering an intuitive view of real-time performance. This visualization highlights how effectively the system detects and orients the marker in various setups.

6.2.1 Overall Performance. Detection Distance. To assess the detection distance of the LiDARMarker, we evaluated the detection rate and accuracy at distances from 7m to 15m. The results, shown in Fig.14(a), indicate a consistent 100% detection rate up to 15m. However, detection accuracy slightly declines, staying above 97% up to 14m and dropping to 94% at 15m. This drop is mainly due to the lower point cloud resolution at greater distances. As the marker moves farther away, fewer LiDAR points are captured, reducing resolution and precision. Additionally, as the distance increases, the laser aperture widens, creating a larger illuminated area per beam. This causes intensity measurement blurring, introducing uncertainty in the decoding process, especially in binary decoding, which relies on clear intensity thresholds. As a result, decoding errors increase at greater distances.

Orientation Estimation. We assess the LiDARMarker’s performance in estimating the marker’s orientation, with the marker placed 9 m from the LiDAR and rotated at different angles. As shown in Fig.14(b), the marker’s orientation is categorized into 8 directions: F, FR, R, BR, B, BL, L, and FL. Detection rate is almost 100% for all orientations, and the orientation accuracy exceeds 97% in all cases. Minor errors in orientation estimation stem from factors like incorrect fitting of the marker in the LiDAR point cloud, which can miscalculate its true orientation. Additionally, IR absorbing coating in the environment can cause random LiDAR measurement errors, introducing noise that affects orientation accuracy.

Distance Estimation. We evaluate distance estimation accuracy across ranges from 7 m to 15 m. The results in Fig.14(c) show the absolute error at different distances. At 7 m, fluctuations occur due to the LiDAR’s limited viewing range, where the marker partially falls outside the sensor’s line of sight at its default height of 1.6 m. This causes incomplete or distorted data, affecting the distance estimation. At around 9 m, increased errors may result from slight misplacement or misalignment of the marker relative to the LiDAR’s field of view. Generally, the error stays below 15 cm up to 14 m but rises significantly to about 24 cm at 15 m, reflecting the reduced precision of LiDAR data at greater distances, as noted in the detection distance evaluation. The estimated error exceeds the LiDAR’s calibration accuracy because the marker’s center falls between adjacent scan lines, making it inaccessible to the LiDAR’s ranging.

Time Consumption. To evaluate the real-time performance of the system, we measure the time consumption of each step in the decoding pipeline, as illustrated in Fig. 14(d). Since the number of LiDAR points associated with the marker varies with distance (decreasing as the distance increases), we evaluated the time consumption at different distances to capture this variation. The results indicate that the time required for the preparation and pattern extraction steps is relatively stable, averaging around 10 ms and 2 ms, respectively. In contrast, the decode and orientation estimation steps are completed in approximately 100ms, with the time consumption decreasing slightly as distance increases. This reduction occurs because fewer LiDAR points are occupied by the marker at greater distances, resulting in decreased computational load during decoding and orientation estimation.

Mobility Test. We evaluated the system on a moving vehicle at speeds from 5 km/h to 45 km/h, excluding frames recorded during acceleration and braking. As shown in Fig. 14(e), the correct rate remains above 90% up to 35 km/h but drops to 76% at 45 km/h.

At lower speeds, vibrations cause frame stretching and truncation, leading to decoding errors. At higher speeds, the restricted detection range (<15 m) yields fewer frames (approximately 13 frames at 40 km/h with a 10 Hz LiDAR refresh rate), thereby reducing opportunities for marker detection and decoding.

Camera-based Method Comparison. We compare the communication range and frame rate of LiDARMarker with a camera-based method using ArUco [33] markers, which are printed on 1.6 m × 1.6 m paper with a 250-code space. The area and payload space of this marker are comparable to LiDARMarker. The decoding algorithm utilizes the built-in OpenCV library [29]. The comparison was conducted under identical lighting conditions, including both daylight and low light, across varying distances. The detection range results, shown in Fig. 14(f), demonstrate that LiDARMarker performs similarly to the camera-based method in daylight but outperforms it under low light conditions. Specifically, LiDARMarker is able to decode the marker at distances of up to 15 m in both daylight and low light, while the camera-based method is only able to detect up to 8 m in low light. In Fig. 14(g), the frame rate comparison shows the camera-based method can achieve at least 85 Hz in daylight, while LiDARMarker can achieve 61 Hz. However, the camera-based method achieves a frame rate exceeding 120 Hz under low light conditions, as the marker pattern is not detected, causing the decoding process to exit immediately.

False Alarm Rate. Evaluations under slightly crowded and heavily crowded traffic yielded FARs of 4.06% and 7.19%, respectively (see Fig. 14(h)). A heavily congested environment has more pedestrians and vehicles and a more complex environment than a lightly congested environment. In heavily crowded conditions, the presence of more vehicles and pedestrians intensifies point cloud noise, heightening the chance of false alarms if random reflections are interpreted as markers.

Summary. In conclusion, the LiDARMarker exhibits excellent performance in terms of detection rate and orientation estimation, with minor degradation in distance estimation accuracy beyond 14 m. This degradation is primarily due to reduced point cloud resolution and the challenges in accurately decoding the marker at longer distances. Furthermore, the system's real-time processing, averaging 15 ms (enabling operation at up to 61 Hz, even though the LiDAR refresh rate is 10 Hz), suits applications that demand high responsiveness.

6.2.2 Impact of parameters. LiDAR's Pitch Angle.

When LiDAR is deployed on a vehicle, the manufacturer may intentionally create a pitch angle for aesthetic reasons or to reduce wind resistance. To evaluate system robustness, we tested the marker detection rate and correct decoding rate at different pitch angles, as shown in Fig. 15(a). The marker was placed at 9 m with the LiDAR installed 0.9 m above the ground. The height was lowered from the standard 1.6 m to ensure the marker remained in the LiDAR's field of view at higher pitch angles. The results show stable performance at pitch angles from -5° to 5°, with both detection and decoding rates exceeding 98%. However, at -2°, performance declined slightly due to a smaller illumination angle and higher laser echo energy, affecting the threshold segmentation method. It is important to note that excessive downward angles reduce the LiDAR's detection range and effective field of view.

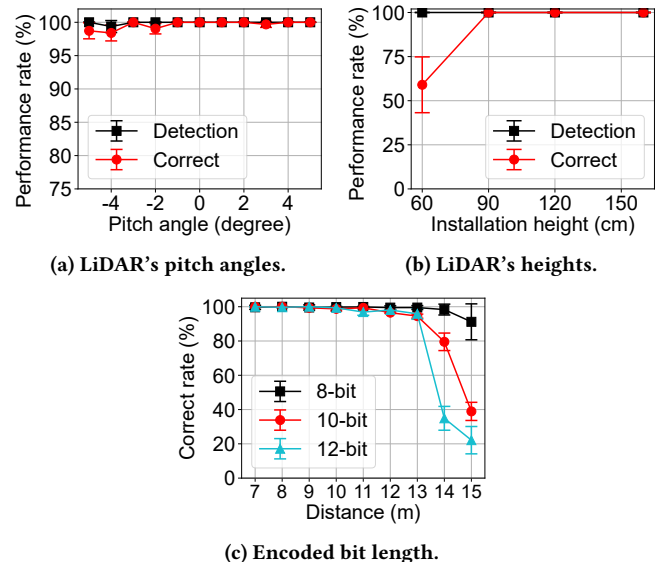
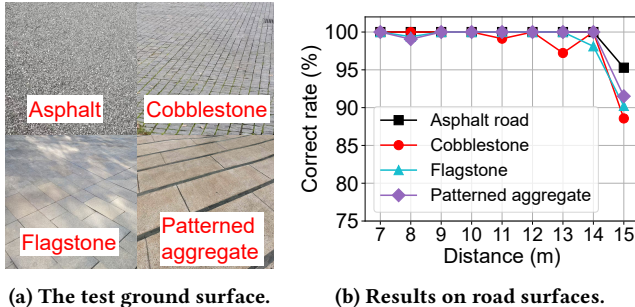


Figure 15: The influence of pitch angle, installation height, and encoded bit length on system performance.

LiDAR's Installation Height. The installation height of the LiDAR is another critical parameter that can affect the system's performance. This evaluation is designed to simulate that the LiDAR is on the roof of some vehicles and below the headlights on others. The results, shown in Fig. 15(b), demonstrate that the system's performance remains stable at installation heights ranging from 0.9 m to 1.6 m. The detection rate and correct rate both keep above 99% at 9 m distance. However, when the installation height is reduced to 0.6 m, the detection rate keep trend but the correct rate has a significant decline. This is because the LiDAR's laser beam is too close to the ground, which causes the intensity difference between the marker and the ground to be too small, making it difficult to distinguish low reflect bars from the ground. Therefore, the system's performance is optimal when the LiDAR is installed above 0.9 m.

Encoded Bit Length. The encoded bit length is another important parameter that can affect the system's performance. The results, shown in Fig. 15(c), demonstrate the system's performance with encoded bit lengths ranging from 8-bit to 12-bit. Longer encoded bit lengths increase the number of bars in the marker, which complicates the decoding process. The primary reason is that a single-bit parity check is insufficient to filter out incorrect decoding results, especially with fewer scanning lines at greater distances. Additionally, more bits reduce the effective working range.

Road Surface Material. Road surface material can affect system performance as different surfaces reflect the LiDAR's laser beams differently. To assess robustness, we tested four common road surfaces: asphalt, cobblestone, flagstone, and patterned aggregate, as shown in Fig. 16(a). The patterned aggregate features stripes with intensity contrast similar to our markers, evaluating the system's anti-interference capability. Results in Fig. 16(b) show reliable performance at shorter distances, with accuracy declining at longer distances, particularly on uneven surfaces like cobblestone. This is due to laser beam scattering on uneven surfaces, which leads to less



(a) The test ground surface.

(b) Results on road surfaces.

Figure 16: Different road surfaces impact on the system's performance.

precise point clouds and reduced decoding accuracy. However, the system maintains stability on asphalt and flagstone, with accuracy above 98% at 14 m. The patterned aggregate surface shows 92% accuracy at 15 m, comparable to other surfaces, indicating that the system is robust on most road surfaces, with slight performance loss on highly textured or uneven ones.

7 Discussion

Work Range, Scenarios, and Potential Improvements. Currently, LiDARMarker is limited to an operational range of 15 m due to three primary factors: 1) LiDAR resolution: An autonomous LiDAR typically provides 128 vertical lines over a 120° field of view with a 0.1° resolution, yielding roughly 128*1200 pixels—about 13.5 times lower than a 1080p camera; 2) Aperture effect: The spreading of the laser beam diminishes its intensity, reducing the contrast between reflective bars and complicating the decoding process; 3) Intensity resolution: With 8-bit data mostly spanning the 0-20 range, the dynamic range is limited, making it challenging to distinguish the encoded bars at extended distances.

Thus, LiDARMarker is best suited for urban environments with low-speed conditions. To boost performance, potential improvements include increasing the LiDAR resolution, correcting for perspective distortions at varying distances, and employing higher-fidelity intensity representations (e.g., 10-bit or floating-point). Additionally, using higher-order modulation schemes (such as FSK or QAM) could enhance both data rates and the decoding range.

Durability. The durability of LiDARMarker primarily depends on its IR absorbing coating. Originally designed for building glass, this coating is resistant to sunlight, water, and abrasion. Research [47] on similar coatings indicates that there is no significant quality degradation after 28 days of water immersion combined with sunlight, thermal, and acid/alkali resistance tests.

Working wavelength. Current IR absorbing coatings are optimized for 905 nm LiDAR infrared, with reduced effectiveness at 1550 nm, potentially causing performance degradation. Nonetheless, it is feasible to develop coatings that strongly absorb at both 905 nm and 1550 nm [45].

8 Related Work

Camera-based marker systems. Fiducial marker systems were initially developed for augmented reality applications [12] and later

adapted to other camera-based scenarios, such as camera parameter correction [8], localization [7], pose estimation [40], and object detection and tracking [34]. Research has focused on improving fiducial markers in terms of usability [19], detection speed [16], accuracy [25], and robustness [16]. With the rise of autonomous driving, fiducial markers have also been used in camera-based autonomous vehicles for navigation, localization, and mapping.

However, camera-based fiducial marker systems have limitations: (i) they are prone to ambient light interference, such as poor visibility in low-light or adverse weather conditions, (ii) they can cause visual pollution when deployed in public areas, and (iii) their detection pipelines are complex and computationally expensive. To address these issues, we propose an invisible marker system with a faster decoding algorithm that leverages LiDAR scanning features.

LiDAR-based marker systems. LiDAR sensors provide 3D coordinates (x, y, z) and reflection intensity i of an object's surface. When an IR laser beam hits an object, the reflection intensity depends on factors like surface material, color, and angle of incidence. A key observation in state-of-the-art systems is that black surfaces, which absorb most IR light, produce low reflection intensities, while white surfaces, which reflect most IR light, produce high reflection intensities. The first LiDAR-based fiducial marker, LiDARTag [16], introduced real-time detection and decoding compatible with AprilTags [28, 37], though it required a dedicated detection zone. Later, Yibo et al. [25] improved detection methods to decode multiple markers integrated into the environment. Other works optimized marker systems by enhancing pose estimation [15] and shape design [39]. For example, Jiunn-Kai et al. [15] optimized marker shapes to reduce pose ambiguity, while A4LidarTag [39] proposed a circular hole pattern to embed localization information via depth differences. However, these systems are limited by operation range (within 1 m) and require high-resolution LiDAR hardware. Despite these advances, LiDAR-based fiducial marker systems face challenges in autonomous driving. First, visible markers cause visual pollution, disrupting driver vision and degrading urban aesthetics. Second, detection and decoding algorithms are computationally intensive. Common pipelines involve clustering, pose estimation, 2D projection, and decoding, processes inherited from camera-based fiducial systems that add significant computational overhead.

Multimodal marker systems. To address the limitations of single sensors, several works propose multimodal fiducial marker systems combining sensors such as cameras, LiDAR, and thermal cameras. Most research focuses on camera and LiDAR fusion for calibration [2, 20, 39, 43, 44] or navigation [6]. ArTuga [4] developed a multimodal fiducial marker system using temperature, reflectivity, and color as coding properties, detectable by thermal cameras, LiDAR, and cameras. However, their marker requires a power supply to maintain temperature differences, making it unsuitable for outdoor environments.

9 Conclusions

In conclusion, we present LiDARMarker, a novel LiDAR marker system designed to address the limitations of traditional markers by leveraging LiDAR's unique imaging and scanning properties. LiDARMarker enables accurate and efficient navigation for autonomous vehicles through its innovative marker design, which

supports real-time decoding and robust orientation estimation. The experimental results demonstrate its effectiveness in improving navigation accuracy, maintaining robustness under varying conditions, and achieving real-time performance with minimal computational overhead.

Acknowledgments

We sincerely thank the anonymous reviewers and our shepherd for their valuable feedback and insightful suggestions, which has greatly strengthened this work. We also extend our gratitude to Yihong Hang for his invaluable support with the experiments. The experiments of this work were supported by the a Core Facility Platform of Computer Science and Communication, SIST, ShanghaiTech University.

References

- [1] Darko Babić, Dario Babić, Hrvoje Cajner, Ana Sruk, and Mario Fiolić. 2020. Effect of road markings and traffic signs presence on young driver stress level, eye movement and behaviour in night-time conditions: a driving simulator study. *Safety* 6, 2 (2020), 24.
- [2] Jorge Beltrán, Carlos Guindel, Arturo de la Escalera, and Fernando García. 2022. Automatic Extrinsic Calibration Method for LiDAR and Camera Sensor Setups. *IEEE Transactions on Intelligent Transportation Systems* 23, 10 (2022), 17677–17689. doi:10.1109/TITS.2022.3155228
- [3] Huaiyu Cai, Weisong Pang, Xiaodong Chen, Yi Wang, and Haolin Liang. 2020. A novel calibration board and experiments for 3D LiDAR and camera calibration. *Sensors* 20, 4 (2020), 1130.
- [4] Rafael Marques Claro, Diogo Brandão Silva, and Andry Maykol Pinto. 2023. Artuga: A novel multimodal fiducial marker for aerial robotics. *Robotics and Autonomous Systems* 163 (2023), 104398.
- [5] Wei Da-chuan. 2010. Algorithm of road information acquirement based on GPS and electronic map. In *2010 3rd International Congress on Image and Signal Processing*, Vol. 9. 4174–4178. doi:10.1109/CISP.2010.5646704
- [6] Spencer Davis, Kenneth G. Ricks, and Ryan A. Taylor. 2019. Reflective Fiducials for Localization With 3D Light Detection and Ranging Scanners. *IEEE Access* 7 (2019), 45291–45300. doi:10.1109/ACCESS.2019.2909467
- [7] César Debeunne and Damien Vivet. 2020. A review of visual-LiDAR fusion based simultaneous localization and mapping. *Sensors* 20, 7 (2020), 2068.
- [8] Ankit Dhall, Kunal Chelani, Vishnu Radhakrishnan, and K Madhava Krishna. 2017. LiDAR-camera calibration using 3D-3D point correspondences. *arXiv preprint arXiv:1705.09785* (2017).
- [9] Dumu. 2024. The HiSilicon SoC-powered Baidu Dumu CM-Mini Panel Has Arrived. [Online] <https://shorturl.at/Dwoua> – Last access: 2024-11-15.
- [10] Margarita Favorskaya and Alexandr Zotin. 2020. Robust textual watermarking for high resolution videos based on Code-128 barcoding and DWT. *Procedia Computer Science* 176 (2020), 1261–1270.
- [11] FHWA MUTCD. 2024. US Road Symbol Signs. [Online] <https://shorturl.at/x7iLY> – Last access: 2024-11-15.
- [12] Thomas Genevois, Jean-Baptiste Horel, Alessandro Renzaglia, and Christian Laugier. 2022. Augmented reality on lidar data: Going beyond vehicle-in-the-loop for automotive software validation. In *2022 IEEE Intelligent Vehicles Symposium (IV)*. IEEE, 971–976.
- [13] Jack Greenhalgh and Majid Mirmehdi. 2012. Real-time detection and recognition of road traffic signs. *IEEE transactions on intelligent transportation systems* 13, 4 (2012), 1498–1506.
- [14] Hesai. 2024. Datasheet. [Online] <https://shorturl.at/1BN4E> – Last access: 2024-11-15.
- [15] Jiunn-Kai Huang, William Clark, and Jessy W. Grizzle. 2022. Optimal Target Shape for LiDAR Pose Estimation. *IEEE Robotics and Automation Letters* 7, 2 (2022), 1238–1245. doi:10.1109/LRA.2021.3138779
- [16] Jiunn-Kai Huang, Shoutian Wang, Maani Ghaffari, and Jessy W Grizzle. 2021. LiDARTag: A real-time fiducial tag system for point clouds. *IEEE Robotics and Automation Letters* 6, 3 (2021), 4875–4882.
- [17] Andrew S Huntington. 2020. *InGaAs avalanche photodiodes for ranging and Lidar*. Woodhead Publishing.
- [18] Margaret Kalacska, J Pablo Arroyo-Mora, and Oliver Lucanus. 2021. Comparing UAS LiDAR and Structure-from-Motion Photogrammetry for peatland mapping and virtual reality (VR) visualization. *Drones* 5, 2 (2021), 36.
- [19] Michail Kalaitzakis, Brennan Cain, Sabrina Carroll, Anand Ambrosi, Camden Whitehead, and Nikolaos Vitzilaios. 2021. Fiducial markers for pose estimation: Overview, applications and experimental comparison of the arttag, apriltag, aruco and stag markers. *Journal of Intelligent & Robotic Systems* 101 (2021), 1–26.
- [20] Kenji Koide, Shuji Oishi, Masashi Yokozuka, and Atsuhiko Banno. 2023. General, Single-shot, Target-less, and Automatic LiDAR-Camera Extrinsic Calibration Toolbox. In *2023 IEEE International Conference on Robotics and Automation (ICRA)*, 11301–11307. doi:10.1109/ICRA48891.2023.10160691
- [21] Liangzhi Li, Kaoru Ota, and Mianxiong Dong. 2018. Humanlike driving: Empirical decision-making system for autonomous vehicles. *IEEE Transactions on Vehicular Technology* 67, 8 (2018), 6814–6823.
- [22] You Li, Pierre Duthon, Michèle Colomb, and Javier Ibanez-Guzman. 2020. What happens for a ToF LiDAR in fog? *IEEE Transactions on Intelligent Transportation Systems* 22, 11 (2020), 6670–6681.
- [23] Dong Liang, Cheng Zhang, Pengfei Zhang, Song Liu, Huijie Li, Shouzhu Niu, Ryan Z Rao, Li Zhao, Xiaochi Chen, Hanxuan Li, et al. 2024. Evolution of laser technology for automotive LiDAR, an industrial viewpoint. *nature communications* 15, 1 (2024), 7660.
- [24] Chunsheng Liu, Shuang Li, Faliang Chang, and Yinhai Wang. 2019. Machine vision based traffic sign detection methods: Review, analyses and perspectives. *Ieee Access* 7 (2019), 86578–86596.
- [25] Yibo Liu, Hunter Schofield, and Jinjun Shan. 2022. Intensity image-based LiDAR fiducial marker system. *IEEE Robotics and Automation Letters* 7, 3 (2022), 6542–6549.
- [26] Kaveh Mirzaei, Mehrdad Arashpour, Ehsan Asadi, Hossein Masoumi, Yu Bai, and Ali Behnood. 2022. 3D point cloud data processing with machine learning for construction and infrastructure applications: A comprehensive review. *Advanced Engineering Informatics* 51 (2022), 101501.
- [27] Jaswanth Nidamanuri, Chinmayi Nibhanupudi, Rolf Assfalg, and Hrishikesh Venkataraman. 2021. A progressive review: Emerging technologies for ADAS driven solutions. *IEEE Transactions on Intelligent Vehicles* 7, 2 (2021), 326–341.
- [28] Edwin Olson. 2011. AprilTag: A robust and flexible visual fiducial system. In *2011 IEEE international conference on robotics and automation*. IEEE, 3400–3407.
- [29] OpenCV. 2025. Detection of ArUco Markers. [Online] https://docs.opencv.org/4.11.0/d5/dae/tutorial_aruco_detection.html – Last access: 2025-2-15.
- [30] Dayong QIAO, Weizheng YUAN, and Yong REN. 2023. Review of MEMS LiDAR. *Microelectronics & Computer* 40, 1 (2023), 41–49.
- [31] Thinal Raj, Fazida Hanim Hashim, Aqilah Baseri Huddin, Mohd Faisal Ibrahim, and Aini Hussain. 2020. A survey on LiDAR scanning mechanisms. *Electronics* 9, 5 (2020), 741.
- [32] Robosense. 2024. Datasheet. [Online] <https://shorturl.at/6yykM> – Last access: 2024-11-15.
- [33] Francisco J Romero-Ramirez, Rafael Muñoz-Salinas, and Rafael Medina-Carnicer. 2018. Speeded up detection of squared fiducial markers. *Image and vision Computing* 76 (2018), 38–47.
- [34] Muhammad Sualeh and Gon-Woo Kim. 2020. Visual-LiDAR based 3D object detection and tracking for embedded systems. *IEEE Access* 8 (2020), 156285–156298.
- [35] Chaopeng Tan and Kaidi Yang. 2024. Privacy-preserving adaptive traffic signal control in a connected vehicle environment. *Transportation research part C: emerging technologies* 158 (2024), 104453.
- [36] Nesrine Triki, Mohamed Karay, and Mohammed Ksantini. 2024. A comprehensive survey and analysis of traffic sign recognition systems with hardware implementation. *IEEE Access* (2024).
- [37] John Wang and Edwin Olson. 2016. AprilTag 2: Efficient and robust fiducial detection. In *2016 IEEE/RSJ International Conference on Intelligent Robots and Systems (IROS)*. IEEE, 4193–4198.
- [38] Xiaoxi He. 2024. Lidar 2024-2034: Technologies, Players, Markets & Forecasts. [Online] <https://shorturl.at/3wlHb> – Last access: 2024-11-15.
- [39] Yusen Xie, Lei Deng, Ting Sun, Yefu Fu, Jian Li, Xinglong Cui, Hanxi Yin, Shuixin Deng, Junwei Xiao, and Baohua Chen. 2022. A4lidartag: Depth-based fiducial marker for extrinsic calibration of solid-state lidar and camera. *IEEE robotics and automation letters* 7, 3 (2022), 6487–6494.
- [40] Dongqiangzi Ye, Yufei Xie, Weijia Chen, Zixiang Zhou, Lingting Ge, and Hassan Foroosh. 2024. LPFormer: LiDAR pose estimation transformer with multi-task network. In *2024 IEEE International Conference on Robotics and Automation (ICRA)*. IEEE, 16432–16438.
- [41] Yole Group. 2024. Automotive LiDAR deployment ramps up in 2024. [Online] <https://shorturl.at/Thf0d> – Last access: 2024-11-15.
- [42] Ekim Yurtseven, Jacob Lambert, Alexander Carballo, and Kazuya Takeda. 2020. A survey of autonomous driving: Common practices and emerging technologies. *IEEE access* 8 (2020), 58443–58469.
- [43] Jun Zhang, Yiyao Liu, Mingxing Wen, Yufeng Yue, Haoyuan Zhang, and Danwei Wang. 2023. L2V2T2Calib: Automatic and Unified Extrinsic Calibration Toolbox for Different 3D LiDAR, Visual Camera and Thermal Camera. In *2023 IEEE Intelligent Vehicles Symposium (IV)*, 1–7. doi:10.1109/IV55152.2023.10186657
- [44] Xinyi Zhang, Shifan Zhu, Shichun Guo, Jun Li, and Huaping Liu. 2021. Line-based Automatic Extrinsic Calibration of LiDAR and Camera. In *2021 IEEE International Conference on Robotics and Automation (ICRA)*, 9347–9353. doi:10.1109/ICRA48506.2021.9561216
- [45] Hong Zhong et al. 2019. Investigation on NIR-shielding multifunctional heat insulation coating materials based on ATO for energy saving of buildings. (2019).

- [46] Husheng Zhou, Wei Li, Zelun Kong, Junfeng Guo, Yuqun Zhang, Bei Yu, Lingming Zhang, and Cong Liu. 2020. Deepbillboard: Systematic physical-world testing of autonomous driving systems. In *Proceedings of the ACM/IEEE 42nd International Conference on Software Engineering*. 347–358.
- [47] Hanwen Zhu, Xiang Li, Qingge Feng, Fanghong Qin, Jing Sun, Shuyu Yuan, Xingyu Deng, Hongxing Zhu, and Ke Xu. 2025. Synthesis of transparent and durable antimony tin oxide coatings based on spectrum-selective transmittance for thermal insulation by regulating dispersion. *Ceramics International* (2025). doi:10.1016/j.ceramint.2025.01.165
- [48] Zhe Zhu, Dun Liang, Songhai Zhang, Xiaolei Huang, Baoli Li, and Shimin Hu. 2016. Traffic-sign detection and classification in the wild. In *Proceedings of the IEEE conference on computer vision and pattern recognition*. 2110–2118.